RSC Advances

PAPER

Cite this: *RSC Adv.*, 2024, **14**, 11633

Enhanced reduction of COD in water associated with natural gas production using iron-based nanoparticles†

Moataz Elsaeed Selim,[a] Magdi E. Khalifa,[a] Fawaz A. Agizah,[b] Eman M. Mostafa[c] and Fathi S. Awad *[ad]

The natural gas production industry faces the problem of the proper disposal of produced water and its treatment with significantly advanced technologies to meet the minimum quality standard for irrigation activities, commercial purposes, and consumption by living organisms. This study describes an effective method for reducing the COD (chemical oxygen demand) content in formation water using different metal oxide nanoparticles such as iron oxide (FO), iron zinc oxide (FZO), and iron vanadium oxide (FVO) nanoparticles. These nanoparticles were synthesized and fully characterized using powder X-ray diffraction (XRD) analysis, Fourier transform infrared (FT-IR) spectroscopy, field emission scanning electron microscopy (SEM), energy dispersive X-ray (EDX) analysis, dynamic light scattering particle size (DLS) analysis and zeta potential analysis. The experimental results revealed that the maximum reduction of COD content was 42.18% using FVO nanoparticles with a dose of 3 g L^{-1} at 25 °C and pH = 6. Compared to commercial products [Redoxy and Oxy(OXYSORB)], the synthesized FO, FZO, and FVO nanoparticles demonstrated their superiority by achieving excellent results in decreasing the COD content of wastewater associated with natural gas production by more than 86%. This study introduces a promising technique for decreasing the COD content using metal oxide nanoparticles, which are eco-friendly, bio-safe, cheap, and nontoxic materials, and improving the quality of wastewater associated with natural gas production for its safe disposal through sewage and treatment plants.

Received 3rd February 2024
Accepted 22nd March 2024

DOI: 10.1039/d4ra00888j

rsc.li/rsc-advances

1. Introduction

Water is the most necessary resource on the planet, and there is no life for humans or any living organism without it. Water has several unique characteristics that make it a precious resource. Today, finding pure water sources is a complicated global problem. Due to an increase in global urbanization and industrialization activities, a large amount of formation water is generated, and this formation water is disposed without proper management and treatment processes.[1] One of these industries is natural gas and oil production, which is facing the problem of disposing the generated formation water and treating it with significantly advanced technologies to meet the minimum quality standard for irrigation activities, commercial purposes, and consumption by living organisms.[2–5] During natural gas exploration and production, the produced fluids consist of natural gas and gas condensates, which are physically separated from formation water using advanced techniques, and the volume of produced formation water depends on the nature and the age of the gas-producing wells.[6] Wastewater associated with petroleum industries (gas/oil) is considered a useless product generated from oil and gas reservoirs. Formation water is in direct contact with exploration petroleum products such as gas and oil in the reservoirs, wells, or surface pipelines. The general properties (chemical and physical) of formation water disposal in the petroleum industry vary greatly depending on the reservoir type (*e.g.*, oil, gas, or coal), the geographic location of the field, geologic formation, and the produced hydrocarbon products (*e.g.*, heavy oil, medium oil, light oil, lean gas, and rich gas). The lifetime of the proposed reservoir is the most critical factor for determining the characteristics and volume of

[a]*Chemistry Department, Faculty of Science, Mansoura University, Mansoura 35516, Egypt. E-mail: fathyawad949@yahoo.com; fathysamy@mans.edu.eg; Tel: +201000166374*

[b]*Rashid Petroleum Company, Cairo, Egypt*

[c]*Production Department, Egyptian Petroleum Research Institute, Cairo, Egypt*

[d]*Chemistry Department, Faculty of Science, New Mansoura University, New Mansoura City, 35712, Egypt*

† Electronic supplementary information (ESI) available: EDX analysis of iron oxide (FO) and iron zinc oxide (FZO) (Fig. S1). DLS analysis of iron oxide (FO) and iron zinc oxide (FZO) (Fig. S2). Zeta potential analysis of iron oxide (FO) and iron zinc oxide (FZO) (Fig. S3). The effect of pH upon % COD reduction at different dosages of nanoparticles (Table S1). The effect of nanomaterial dosage (upon % COD reduction (Table S2). The effect of temperature upon % COD reduction (Table S3). The effect of different commercial products upon % COD (Table S4). The components of oilfield water (Table S5). The ICSD of compounds existed in FO nanomaterials (Fig. S4). The ICSD of compounds existed in FZO nanomaterials (Fig. S5). The ICSD of compounds existed in FVO nanomaterials (Fig. S6). See DOI: https://doi.org/10.1039/d4ra00888j

formation water associated with petroleum industries, in which the small amount of formation water products at the beginning of the production from the reservoir increases with time as the reservoir becomes older.[7]

Formation water produced in the natural gas industry is considered contaminated water compared with ground and surface water, which contains various organic species such as dissolved and dispersed hydrocarbons, phenols, and aromatic compounds, in addition to inorganic matter such as minerals, gases, heavy metals and biological contaminants such as SRB (sulfate reducing bacteria).[7] The composition of formation water associated with natural gas production depends on the geological age and location, field position, type of production wells, and chemicals used during the production process, such as corrosion inhibitors, methanol, mono ethylene glycol, and biocides.[8,9] Also, it has abnormal values in salinity, alkalinity, Chemical Oxygen Demand (COD), and Biochemical Oxygen Demand (BOD). Discharging the formation water in natural water sources without effective treatment will be toxic to living organisms and have harmful impacts on the environment.[2,10–13] Formation water produced by the petroleum industry contains large quantities of pollutants that can badly affect the components of the environment, including human health, different water resources, air, crop production, aquatic life, *etc.* In addition, formation water from gas production is more toxic than that produced from oil because it contains high contents of hydrocarbons such as benzene, toluene, and xylene, which causes many problems such as dehydration and death of plants due to high salinity and damage to aquatic species because of reducing oxygen level (high levels of COD and BOD), scale problem and environmental impact due to chemical additives like corrosion inhibitors, methanol and biocides.[14,15]

The COD value of the wastewater is the most critical parameter for ensuring the quality of wastewater for disposal and the monitoring/control of discharge. The COD is an indicator of the concentration of organic constituents present in the wastewater.[16,17] In recent years, the importance of treatment and reusing the formation water has increased by using advanced treatment techniques for reducing the values of COD, BOD_5, oil and grease, and TSS to acceptable levels for using water for different purposes. In the petroleum industry, the removal of hydrocarbon components is the main aim in the treatment of formation water associated with the petroleum industry. There are many techniques (chemical, physical and biological) that are used in formation water treatment, such as chlorine and its derivatives, ultraviolet light,[18] boiling, low-frequency ultrasonic irradiation,[17,19] distillation, reverse osmosis, water sediment filters (fiber and ceramic), activated carbon, solid block, pitcher and faucet-mount filters, bottled water, ion exchange water softeners, flotation, coagulation and ozonisation. There are many factors in choosing the most effective method and the suitable materials for formation water treatment, such as its efficiency, reuse of the materials used, environmentally friendly materials, and cost-effectiveness.[20–22] Although chemical and physical methods are preferred, they have some disadvantages, such as the high cost of treatment and massive, hazardous sludge produced from chemical treatment.[23,24]

In the recent century, nanotechnology has become the most unique and advanced technology that has helped humans solve several problems related to the environment and industry. This technology has many technical applications in science,[25] such as nano system physics,[26] nano chemistry,[27] nanomaterials science, nanobiology,[28] nanoelectronics,[25] nano processing[25] and nano mechanics.[25] Nanomaterials are defined as materials that have dimensions less than 100 nm.[29,30] Due to their existence on the nanoscale, nanomaterials have unique properties better than those of microscale materials, such as adsorption, small size, high surface area, reactivity, and catalytic activities.[20,31] Nanomaterials have many applications in different fields, such as pharmaceuticals, medicine, photocatalysts, formation water treatment, removal of pollutants, and sensors.[29] Many nanomaterials, such as titanium oxide nanoparticles, iron oxide nanoparticles, silver nanoparticles, zinc oxide nanoparticles, vanadium oxide nanoparticles, and copper nanoparticles,[32,33] are used in formation water treatment.

In this research, metal oxide nanoparticles such as iron oxide (FO), iron zinc oxide (FZO), and iron vanadium oxide (FVO) nanoparticles were used to reduce the COD content in the formation water. The factors affecting the process of decreasing COD content using the metal oxide nanoparticles were studied to reach optimum conditions to achieve the maximum reduction of COD content, and these factors are nanoparticle concentration, temperature, and pH. These metal oxide nanoparticles are synthesized using the green synthesis method. The advantages of the green synthesis method are using eco-friendly, bio-safe, cheap, and nontoxic materials, availability of starting materials, and an effortless synthesis method. The pollutants and waste from this technique are the lowest waste compared to other synthesis techniques. This study introduces a promising, effective method to decrease the COD content and improve the quality of wastewater associated with natural gas production for disposal in sewage treatment plants. It reveals that using nanomaterials in wastewater treatment is an effective and distinctive method compared to other traditional treatment methods because of their unique properties, such as high surface area, small size, surface modifiability, magnetic properties, and excellent biocompatibility.

2. Materials and experimental

2.1. Materials and reagents

Iron chloride ($FeCl_3$ and $FeCl_2$), plant extract (green tea extract), sodium hydroxide (NaOH), distilled water, ammonium vanadate, anhydrous zinc chloride, and ammonia solution were obtained from Sigma-Aldrich. Commercial products [Redoxy and Oxy(OXYSORB)] were purchased from Watch Water company. Industrial formation water was obtained from a natural gas production company mercury(II)sulfate was obtained from scholar company.

The samples of the formation water (2 L) were collected from the sampling point of the industrial formation water tank at the natural gas production plant. The collection of samples was carried out using suitable glass containers and standard sampling procedures. All chemicals used in this research were

of analytical grade and had the highest purity. All solutions were prepared in distilled water and made on each experimental day.

2.2. Experimental

2.2.1. Synthesis of iron oxide (FO) nanoparticles. Iron oxide (Fe_3O_4 and Fe_2O_3) nanoparticles were synthesized through a green approach using a single-step method. A 0.01 M solution of iron chloride ($FeCl_3$ and $FeCl_2$) was combined in a sterile flask with an equal volume of green tea leaf extract. The plant extract was introduced into the iron chloride solution under constant stirring for 1–2 hours. The plant extract comprises a variety of biomolecules such as carbohydrates, amino acids, flavonoids, proteins, saponins, terpenoids, and nitrogenous compounds that act as reducers, stabilizers, redox mediators, and capping agents in the synthesis of nanoparticles.[34] A sodium hydroxide solution was employed to adjust the pH of the solution to 10. Subsequently, the resulting solution underwent centrifugation, and the supernatant was removed. The iron oxide nanoparticles were washed with distilled water and subjected to another round of centrifugation to eliminate any remaining impurities. The obtained powder underwent calcination at 500 °C for four hours with concurrent drying at 100 °C.

2.2.2. Synthesis of iron zinc oxide (FZO) nanoparticles. The mixed-phase iron zinc oxide (Fe_2O_3–ZnO) nanoparticles were fabricated. A solution was prepared by dissolving 10 grams of anhydrous zinc chloride in distilled water. Subsequently, ammonia solution was added drop by drop to an actively stirred solution containing 40 grams of anhydrous ferric chloride in distilled H_2O, and maintained at 80 °C. The reaction mixture, continuously stirred with a magnetic stirrer, underwent a four-hour heating process at pH 9. After sufficient precipitation, the resultant material was centrifugated and thoroughly washed with distilled water to eliminate ammonium ions. The washed material was then dried at 100 °C. The final step involved calcination of the powder at 500 °C for four hours.[35]

2.2.3. Synthesis of iron vanadium oxide (FVO) nanoparticles. Iron vanadium oxide ($FeVO_4$) nanoparticle synthesis uses a straightforward one-step method. Initially, a solution was prepared by dissolving 20 grams of ammonium vanadate in distilled water. The ammonia solution was subsequently added dropwise to a vigorously stirred solution containing 160 grams of anhydrous ferric chloride in distilled H_2O at 80 °C. The reaction mixture was heated and stirred continuously using a magnetic stirrer for four hours. The reaction vessel was left undisturbed overnight at room temperature after complete precipitation. The resulting solid was then filtered and subjected to centrifugation, with repeated washing using distilled water to remove ammonium ions. Subsequently, the material was dried at 100 °C and calcined for four hours at 500 °C. FO, FZO, and FVO designations represent iron oxide, iron zinc oxide, and iron vanadium oxide, respectively.

2.2.4. Instrumentations. The FO, FZO, and FVO NPs were characterized for elemental identification and quantitative compositional information using powder X-ray diffraction (XRD) using (Bruker, Germany) operated at 40 kv and 40 mA using Cu ka radiation (1.54060 Å). The Fourier transform infrared (FT-IR) spectra of NPs were recorded using a Fourier transform infrared spectrometer (JASCO FT/IR- 4600 typeA) in the range of 4000–400 cm^{-1} with a resolution of 1.0 cm^{-1}. The surface morphology of (FO, FZO, and FVO) NPs was characterized by field emission scanning electron microscopy (SEM, Quanta FEG 250 with field emission gun, FEI Company, Netherlands). The particle size distribution in the solution and the mean size of the synthesized NPs were studied using dynamic light scattering particle size (DLS) analysis (Malvern, UK). The state of the nanoparticle's surface and stability of a colloidal dispersion were studied using zeta potential analysis (Malvern, UK). The equipment used in this experiment is a digital balance, water bath, pHep by HANNA, digital thermometer, COD Reactor by HANNY, and DR/3900 spectrophotometer by HACH.

2.2.5. COD removal experiments. The COD value of the formation water (wastewater associated with natural gas production) is the most critical parameter for ensuring the quality of the formation water for disposal and the monitoring/control of discharge. The COD indicates the concentration of organic constituents present in formation water. The experiments were carried out to reach optimum conditions and achieve the maximum reduction of COD content using the three types of nanoparticles (FO, FZO, and FVO). The efficiency of reducing COD was studied at different doses (1.5 g L^{-1}, 3 g L^{-1}, and 4.5 g L^{-1}), at different pH values (3, 4, 6, 8, and 10), and at different temperature values (25 °C, 30 °C, 40 °C, 50 °C and 60 °C). The prepared formation water samples were stirred for 1 hour (150 rpm), and the upper part of the treated sample was used to measure COD values. The COD analysis was conducted using the HACH method 8000 and USEPA reactor digestion method (HR Plus), using high-range vials (1000–10000 mg L^{-1}) and the HACH Odyssey DR/3900 spectrophotometer manual. The removal efficiency of the COD was calculated using equation.[36]

$$P = \frac{C_i - C_o}{C_i} \times 100\%$$

where P(%) is the removal percentage of COD; C_o is the initial concentration of COD (mg L^{-1}); C_i is the final concentration of COD (mg L^{-1}).

3. Results and discussion

3.1. Characterization of iron oxide (FO), iron zinc oxide (FZO) and iron vanadium oxide (FVO) nanoparticles

The results of the XRD analysis of FO nanomaterials showed the peaks of the corresponding XRD patterns which are referenced to the following compounds, as shown in Fig. 1A. The hexagonal hematite Fe_2O_3 shows diffraction peaks at 24.120°, 33.077°, 35.627°, 40.820°, 49.401°, 53.945°, 57.429°, 62.381°, 63.993°, 71.661° and 75.445° corresponding to (012), (104), (110), (113), (024), (122), (214), (030), (1010) and (220) patterns, respectively. The cubic magnetite Fe_3O_4 shows diffraction peaks at 18.292, 21.152° and 35.439° corresponding to (111), (002), and (113) patterns, respectively.[36,37] Fig. S4† shows the ICSD of the above compounds.

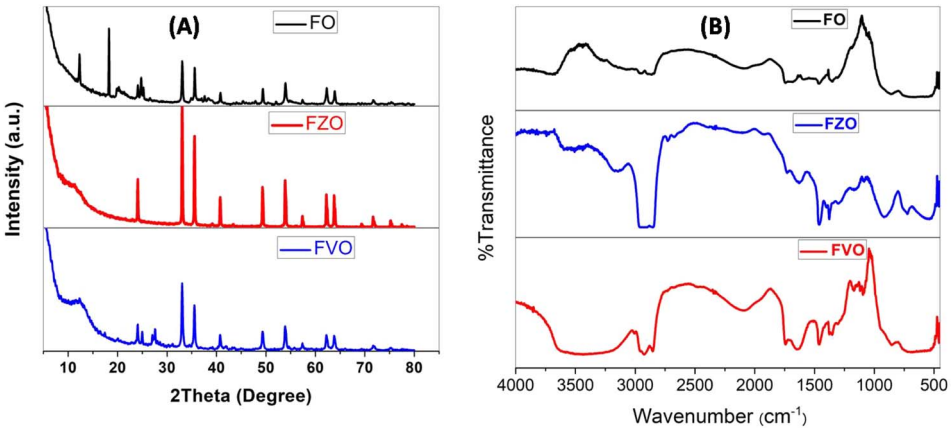

Fig. 1 XRD analysis (A) and FT-IR spectra (B) of iron oxide (FO), iron zinc oxide (FZO), and iron vanadium oxide (FVO) nanoparticles.

The XRD analysis of FZO nanomaterials showed many peaks of XRD patterns related to the following compounds as shown in Fig. 1A: hexagonal hematite $Fe_{1.766}O_3$ shows diffraction peaks at 24.120°, 33.077°, 35.627°, 39.129°, 40.820°, 43.488°, 49.401, 53.945°, 57.429°, 62.381°, 63.993°, 69.406° and 71.661° corresponding to (012), (104), (110), (006), (113), (202), (024), (116), (122), (030), (208) and (1010) patterns, respectively, cubic magnetite Fe_3O_4 shows diffraction peaks at 35.509°, 43.157° and 75.162° corresponding to (113), (004), and (226) patterns, respectively, hexagonal hematite $Fe_{36}O_{36}$ shows diffraction peaks at 32.958°, 38.240°, 51356°, 54.250°, 58.856°, 61.513°, 62.384, 69.129°, 72.2.385°, and 74.789° corresponding to (110), (012), (202), (211), (300), (113), (122), (220), (104), and (131) patterns, respectively, cubic magnetite Fe_3O_4 shows diffraction peaks at 35.659°, 43.341°, 53.778°, and 57.331° corresponding to (113), (004), (224), and (115) patterns, respectively, cubic magnetite $Fe_{2.937}O_4$ shows diffraction peaks at 35.279°, and 62.241° corresponding to (113), and (044) patterns, respectively, and ZnO shows diffraction peaks at 31.9°,34.6° and 36.2° corresponding to (100), (002) and (101) patterns, respectively.[37,38] Fig. S5† shows the ICSD of the above compounds.

The XRD analysis of FVO nanomaterials indicated many peaks of XRD patterns related to the existing compounds as shown in Fig. 1A: hexagonal hematite (water containing) $H_{0.99}Fe_{1.67}O_3$ shows diffraction peaks at 24.113°, 33.080°, 35.605°, 40.806°, 43.465°, 49.386°, 53.945°, 57.413°, 62.354°, 63.950°, 71.694° and 75.392° corresponding to (012), (104), (110), (113), (202), (024), (116), (018), (214), (030), (1010) and (220) patterns, respectively, orthorhombic vanadium oxide hydroxide $H_{0.3}O_2V_1$ shows diffraction peaks at 27.585°, 55.473°, and 75.303° corresponding to (110), (211), and (320) patterns, respectively, tetragonal vanadium oxide hydroxide $O_{0.532}V_1$ shows diffraction peaks at 40.019° and 43.497° corresponding to (011) and (110) patterns, respectively, tetragonal vanadium oxide O_2V_{16} shows diffraction peaks at 40.675° and 42.734° corresponding to (042), and (440) patterns, respectively, and monoclinic vanadium oxide O_7V_3 shows diffraction peaks at 24.926° and 31.261° corresponding to (111), and (206) patterns, respectively.[29,32] Fig. S6† shows the ICSD of the above compounds. The average sizes of the nanoparticles have been estimated from the full width at half maximum (FWHM) of the diffraction peak using the Debye-Sherrer formula according to the equation

$$D = k\lambda/\beta \cos\theta$$

where D is the crystallite size, k is the shape factor (≈ 0.9), λ is the X-ray wavelength (1.540 Å), β is the full-width at half maximum (FWHM) in radians, and θ is the Bragg diffraction angle value. The mean sizes of FO, FZO, and FZO nanoparticles are 45.22 nm, 84.58 nm, and 44.64 nm, respectively.

Fig. 2B illustrates the FTIR spectrum of FO, FZO, and FVO nanoparticles. In the FTIR spectrum of FO nanoparticles, the absorption bands are observed from the FTIR spectrum at 3439 cm^{-1}, 469.582 cm^{-1}, 436.798 cm^{-1}, and 421.37 cm^{-1}. A broad band appears at 3439 cm^{-1} due to –OH stretching, and the Fe–O bond vibration of Fe_3O_4 nanoparticles is at 469.582 cm^{-1}. The low-frequency band at 436.798 cm^{-1} can be related to the Fe–O deformation in the octahedral region of hematite. A peak at 421.37 cm^{-1} shows the Fe_2O_3 bending vibration.[34,35] From the FTIR spectrum of FZO nanoparticles, the absorption band is observed at 3498 cm^{-1}, 539.971 cm^{-1}, 480.188 cm^{-1}, 469.582 cm^{-1}, 436.798 cm^{-1}, and 420 cm^{-1}. A broad band appears at 3498 cm^{-1} due to –OH stretching, and the Fe–O bond vibration of Fe_3O_4 nanoparticles is at 469.582 cm^{-1}. The low-frequency band at 436.798 cm^{-1} can be related to the Fe–O deformation in the octahedral region of hematite. The peak at 421.37 cm^{-1} shows the Fe_2O_3 bending vibration. The strong peaks at 539.971 and 480.188 cm^{-1} correspond to the stretching vibrations of Zn–O bands, which indicates that the samples are well crystallized.[35,36] From the FTIR spectrum of FVO nanoparticles, the absorption bands are observed at 3436.53 cm^{-1}, 1024.98, 468.617 cm^{-1}, 436.798 cm^{-1}, and 420.4 cm^{-1}. A broad band appears at 3436.53 cm^{-1} due to –OH stretching, and the Fe–O bond vibration of Fe_3O_4 nanoparticles is at 468.617 cm^{-1}. The low-frequency band at 436.798 cm^{-1} can be related to the Fe–O deformation in the octahedral region of hematite. The peak at

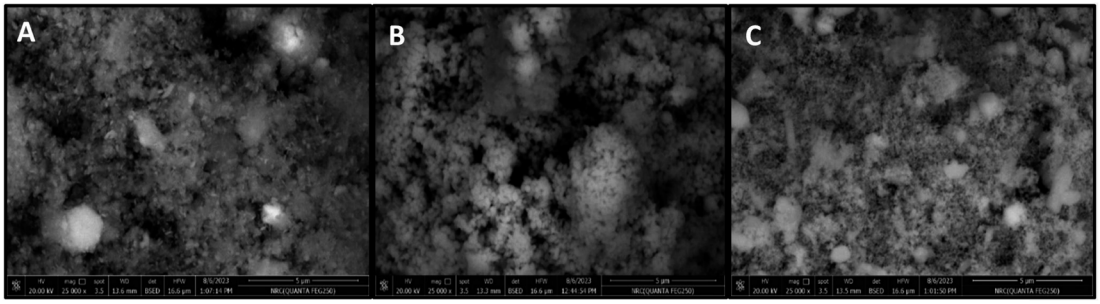

Fig. 2 SEM images of iron oxide (FO) (A), iron zinc oxide (FZO) (B), and iron vanadium oxide (FVO) nanoparticles.

420.4 cm $^{-1}$ shows *vs.* (symmetric stretching) modes of V–O–V vibration and the peak observed around 1024.98 cm^{-1} is attributed to the terminal oxygen vibration mode (V=O).[39,40]

The SEM images (Fig. 2) showed the morphology and the successful synthesis of FO, FZO, and FVO nanoparticles. The particle sizes of FO, FZO, and FVO nanoparticles are 254 nm, 290 nm, and 232 nm, respectively.

The EDX results showed the successful synthesis of FO, FZO, and FVO nanoparticles. From the EDX spectrums, the elemental analysis of samples reveals that iron oxide (FO) nanoparticles contain 39.28% iron weight and 60.72% oxygen weight as shown in Fig. S1(A),† iron zinc oxide (FZO) nanoparticles contain 84.16% iron weight, 9.75% oxygen weight and 6.09% zinc weight as shown in Fig. S1(B)† and iron vanadium oxide (FVO) nanoparticles contain 70.56% iron weight, 13.25% oxygen weight and 16.19% vanadium weight as shown in Fig. 3. The EDX analysis confirms the presence of FO, FZO, and FVO nanoparticles.

Fig. S3† shows the zeta potential of FO nanoparticles and FZO nanoparticles. The zeta potential value of iron oxide (FO) nanoparticles is −21.6 mV, the zeta potential value of iron zinc oxide (FZO) nanoparticles is 14.1 mV, and the zeta potential value of iron vanadium oxide (FVO) nanoparticles is −23.6 mV as shown in Fig. 4B. The zeta potential value far from zero indicates that the particles disperse well in the media since the electrostatic repulsive force among the particles is significant. Thus, the particles have high aqueous stability. The nanoparticle dispersion with a value of zeta potential far from zero indicated stable or relatively high monodispersion, while that with a value close to zero indicated poor monodispersion. The particles with the zeta potential close to zero agglomerate to minimize Gibbs free energy. Surface modification by zinc or vanadium could prevent particle agglomeration and enable the dispersion of individual particles in the media.[41]

3.2. COD removal results

The effect of pH value on reducing COD content in formation water associated with natural gas production was studied by using FO, FZO, and FVO at different solution pH values (3, 4, 6, 8, and 10) and different doses of nanoparticles (1.5, 3.0, and 4.5 g L^{-1}) at room temperature. The effect of pH on the adsorption behavior of different nanomaterials (FO, FZO, and FVO) for reducing the COD content is shown in Table S1† and Fig. 5. The optimum solution pH was 6 for FVO and FZO and 8 for FO, which achieved the highest adsorption capacity for reducing the COD. The pH of the solution regulates the adsorption capacity because it affects the adsorbent's surface

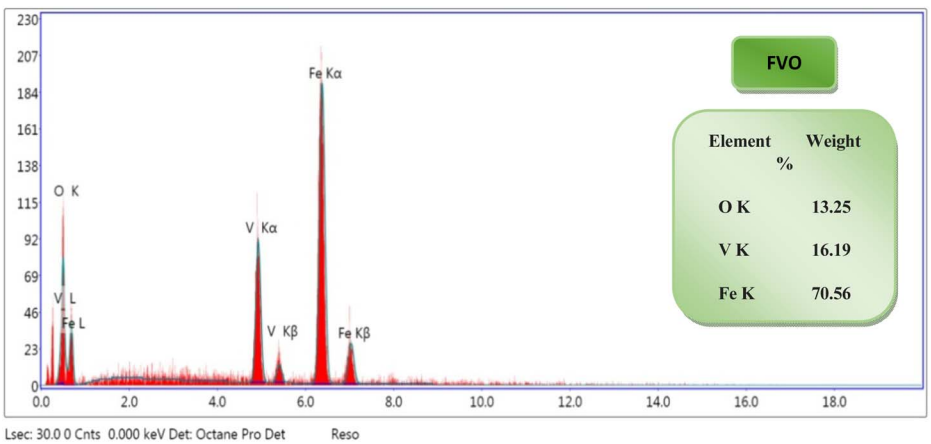

Fig. 3 EDX analysis of iron vanadium oxide (FVO) nanoparticles. The results of DLS analysis for FO, FZO, and FVO nanoparticles are presented in Fig. 4A and S2,† including size distribution by number. The mean hydrodynamic sizes of iron oxide (FO), iron zinc oxide, and iron vanadium oxide (FVO) nanoparticles are 426.4 nm, 487.7822 nm, and 330.9 nm, respectively.

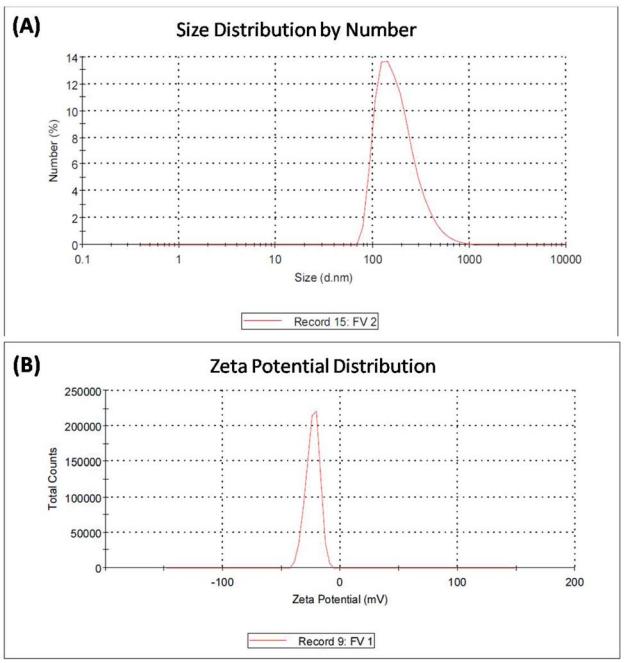

Fig. 4 DLS analysis (A) and zeta potential analysis (B) of iron vanadium oxide (FVO) nanoparticles.

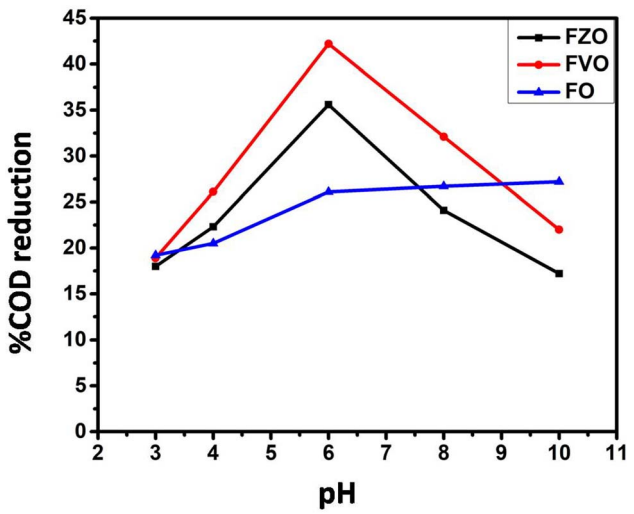

Fig. 5 The effect of pH upon % COD reduction using FO, FZO, and FVO at 3.0 g L^{-1} and 25 °C.

characteristics. The adsorption capacity for nanomaterials decreased at low values (acidic medium) because positively charged hydrogen ions and organic contaminants repel each other electrostatically. When there is a significant concentration of H^+, organic contaminants are substituted by protons at the adsorbent site, which decreases the removal efficiency. The stability of iron oxides decreases in an acidic medium. However, the adsorption capacity of nanoparticles improved as the pH values were raised from 3 to 6. Since fewer hydrogen ions were present at this pH, the functional groups on the adsorbent binding site were free to bond with organic contaminants and potentially produce organic pollutant–chelate complex. The percentage of COD content removal reduced at high pH levels (pH > 6). The competition between OH^- ions and organic pollutants for adsorption sites on the adsorbent surface causes a decrease in organic pollutant removal at a pH above the ideal pH.[42]

The effect of adsorbent dosage on reducing COD content by three different nanoparticles FO, FZO, and FVO in formation water associated with natural gas production was studied by carrying out experiments with different doses (1.5, 3.5, and 4.5 g L^{-1}) at pH 6 and 25 °C. The effect of adsorbent dosage on the adsorption behavior of FO, FZO, and FVO nanomaterials for reducing COD content is shown in Table S2† and Fig. 6A. The COD removal efficiency increased with increasing adsorbent doses (1.5 to 3 g L^{-1}) because more adsorption sites were available on the adsorbent surface, increasing surface area and adsorption capacity. However, the COD removal efficiency decreased at the adsorbent dose of 4.5 g L^{-1} because of the aggregation of nanomaterials, which reduced the total surface area and adsorption capacity. The maximum COD content reduction was achieved at 3 g L^{-1} for FO, FZO, and FVO nanomaterials.[43–45]

The effect of temperature value on reducing COD content by three different nanoparticles (FO, FZO, and FVO) in formation water associated with natural gas production was studied by carrying out experiments at different temperatures (25 °C, 30 °C, 40 °C, 50 °C, and 60 °C), 3 g L^{-1} dosage and pH 6. The effect of temperature on the adsorption behavior using different nanomaterials (FO, FZO, and FVO) for reducing COD content is shown in Table S3† and Fig. 6B. The highest COD removal was at 25 °C for all nanomaterials. The efficiency of reducing COD content decreased with increasing the temperature above 25 °C. So, the nature of the adsorption is exothermic.[46] The temperature scale was chosen to match and reflect the conditions of normal operations at natural gas production sites, which are limited between 25 °C and 60 °C. In addition to increasing temperatures, it will represent an economic burden and a high significant cost. The use of heat exchangers on site to change and control temperatures could be an essential objective to apply. The primarily goal is to treat the wastewater operationally and economically appropriately.

The effect of commercial products on % COD reduction was studied by experimenting with two commercial products (Redox and Oxy) at different dosages (1.5, 3.0, 4.5, 100.0, 200.0, and 300.0 g L^{-1}). The results revealed that the maximum COD reduction (22.12%) was obtained using the commercial product Redoxy at 300 g L^{-1}, 25 °C, and pH = 10. In comparison, 0.0% COD reduction is achieved using the commercial product Oxy under the same experimental conditions, as shown in Table S3.† Therefore, FO, FZO, and FVO nanomaterials are highly efficient in reducing COD content in formation water samples compared to commercial materials. This is because they work at any pH value, are environmentally friendly, and can reduce COD content by more than 86% when compared to commercial products, which can only be used in alkaline medium (pH = 10). Fig. 7 compares the commercial products and nanoparticles (FO, FZO, and FVO).

3.3. The mechanism of COD removal in oilfield water using nanoparticles (FO, FZO, and FVO)

The oxidation power of the used nano compounds (according to the oxidation efficiency) in decreasing COD content varies and can be arranged as follows: FVO > FZO > FO > Redox > Oxy. For FVO nanoparticles, their power of decreasing COD content could be explained by the zeta potential value of −23.6 mV, in which the electrostatic repulsive force among the particles is largest and those particles have the most considerable aqueous stability compared to the zeta values for the other nanoparticles (FO and FZO). Additionally, the FVO NPs have high adsorption capacity due to their small particle size (232 nm) compared to other nanoparticles, which increases their surface area and efficiency in removal and decreases the COD content. The FVO is the most effective nanoparticle. Moreover, the photocatalytic behavior of FVO is mostly the effective force in the photocatalytic degradation of the organic pollutants in water formation. Thus, FVO can have a higher photo catalyst absorption of visible light than the other two compounds, FZO and FO.[47,48]

$H_{0.99}Fe_{1.67}O_3 + h\nu \rightarrow H_{0.99}Fe_{1.67}O_3$ (ecb^-, h_{vb}^+)

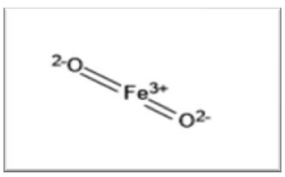

Iron(III) hydrogen oxide

$H_{0.3}O_2V_1 + h\nu \rightarrow H_{0.3}O_2V_1(ecb^-, h_{vb}^+)$

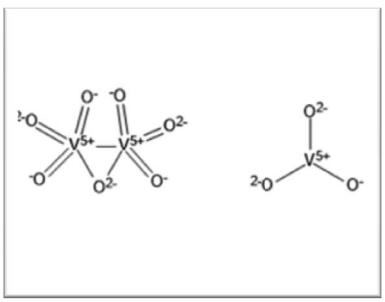

Vanadium oxide hydroxide

$V_2O_5 + h\nu \rightarrow V_2O_5(ecb^-, h_{vb}^+)$

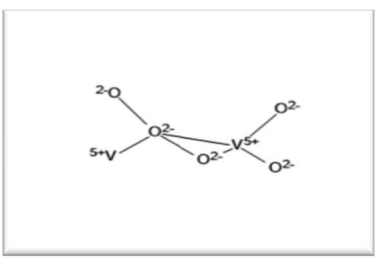

Vanadium oxide

Iron oxides mainly acted as a photocatalyst, while organic pollutants existing in the formation water, like mono ethylene glycol and methanol, which are the leading cause of high COD content, will generate electron–hole pairs, and the heterogeneous iron oxide–glycol/methanol medium (system) could exhibit a robust ligand-to-metal charge transformation ability as described below. Firstly, glycol/methanol can be adsorbed by iron oxide particles to form iron oxide–glycol/methanol complexes on the surface in solution, which are much more photoactive than other Fe^{3+} species, with the generation of methanol radical and glycol radical. Then a rapid decarboxylation is followed, and glycol radical is transformed into carbon-centered radical $CO_2^{\bullet-}$, and then further transformed into superoxide ion ($CO_2^{\bullet-}$) radical, which produces H_2O_2 and O_2 by disproportion. H_2O_2 plays an essential role in the photocatalytic degradation process. The photo-Fenton-like system (Scheme 1) can be considered a promising and effective method for the photocatalytic degradation of organic pollutants and achieves excellent results in removing organic contaminants.[48,49]

Generally, the oxidation power of the used iron oxide nanomaterial compounds varied widely in the purification of the industrial formation water from one to another due to the influence of the physical properties of contaminants that existed in the water rather than the properties of nanomaterials themselves, such as the size of nanomaterials, adsorption characters of the NMs, mechanism of the nanomaterials and photocatalytic behaviors. Therefore, the difference in the size of Fe_3O_4 nano adsorbents was favorable for the diffusion of metal ions from water solution onto the active sites of the adsorbent surface of nanomaterials. Fe_3O_4 nanomaterials are adequate for rapidly removing and decreasing metal ions from industrial water effluents.[48,50,51]

The adsorption mechanism of contaminants from industrial water by modified iron oxide nanoparticles includes surface site binding, magnetic selective adsorption, electrostatic interaction, and a combination of modified ligands. Thus, the addition of specific metal ions of heavy transition metals to the nanomaterials can achieve high efficiency in the oxidation operation of COD content existing in the formation water. The adsorption of organic contaminant species that existed in the formation water took place *via* surface exchange reactions until the surface functional sites were fully occupied, and the other contaminants could diffuse into the adsorbent for further interactions with the functional groups in the nanoparticles. So, modification and chemical treatment using NMs can be widely used to enhance the adsorption capability target. The important information obtained from this research is a precious aspect that is overcoming the toxicity of magnetic nano compounds generally synthesized by nanotechnology. The synthesis of nontoxic nanomaterials *via* green chemistry almost diminishes the environmental pollution as much as possible. It gives a better understanding of the potential hazards that can be mitigated using magnetic nanomaterials, especially in water and wastewater treatment.

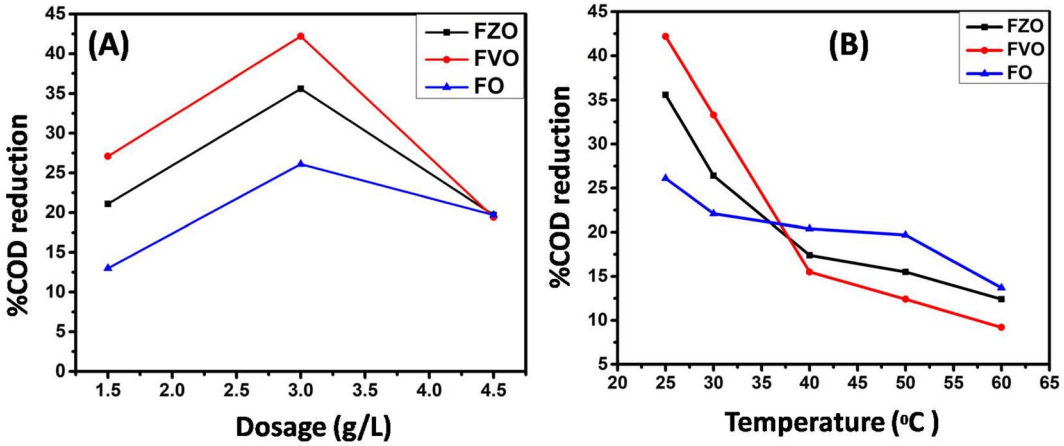

Fig. 6 (A) The effect of nanomaterial dosage (1.5, 3.0, and 4.5 g L^{-1}) upon %COD reduction at pH 6; (B) the effect of different temperatures (25 °C, 30 °C, 40 °C, 50 °C and 60 °C) upon % COD reduction at a dose of 3 g L^{-1} of nanomaterials.

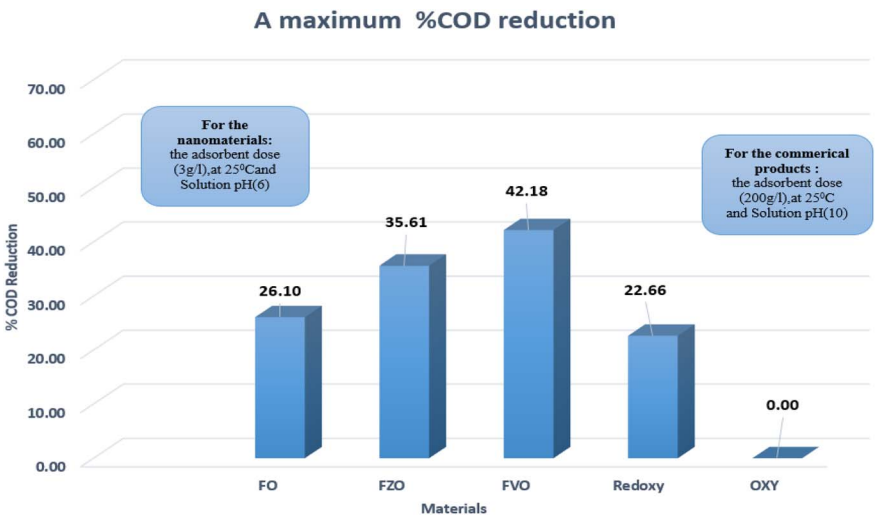

Fig. 7 The maximum % COD reduction for commercial products (Redoxy and Oxy) and synthesized nanomaterials (FO, FZO, and FVO).

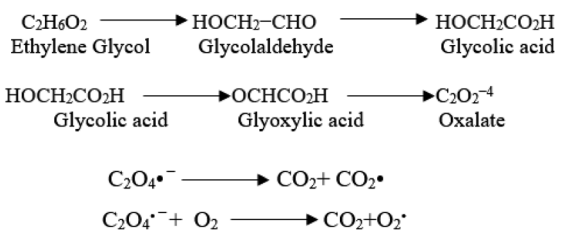

Scheme 1 The photo-Fenton-like system is an effective method for photocatalytic degradation of organic pollutants.

4. Conclusion

This study described a promising attempt to reduce the COD levels in the formation water associated with natural gas production using iron-based nanoparticles such as iron oxide (FO) NPs, iron zinc oxide (FZO) NPs and iron vanadium oxide (FVO) NPs. The synthesized FO, FZO, and FVO nanoparticles were characterized by different techniques such as XRD, FT-IR, SEM, EDX, DLS, and zeta potential analysis. Many factors such as concentration, pH, and temperature are studied to get optimum conditions to achieve the most efficiency of % COD reduction using nanoparticles synthesized by a simple method in one step. The results illustrated that the optimum conditions for achieving the maximum COD content reduction by different nanomaterials (FO, FZO, and FVO) are 3.0 g L^{-1} adsorbent dose, 25 °C, and pH (6). The highest percentages of COD content reduction are 26.10% for FO, 35.61% for FZO, and 42.18% for FVO. Compared to commercial products (Redoxy and Oxy), the synthesized FO, FZO, and FVO nanoparticles have demonstrated their superiority by achieving excellent results in decreasing the COD content of formation water by more than 86%. With a COD reduction rate of up to 42.18% compared to other materials, iron vanadium oxide (FVO) is considered the best nanomaterial utilized overall. The chemical removal of COD using green synthesized nanomaterials was one of the

biggest challenges in selecting and applying it to wastewater treatment operations. However, the obtained 42.18% COD removal represents an excellent result for COD removal from the chemical treatment plant objective point of view; the additional requirements for treatment could be achieved by the suitable chemical treatment and/or powerful oxidation operations such as ozonisation.

Conflicts of interest

There are no conflicts to declare.

Acknowledgements

This paper is based upon work supported by mansoura university research fund.

References

1 M. Amjad, S. Hussain, K. Javed, A. R. Khan and M. Shahjahan, *World*, 2020, **5**, 34–40.
2 S. Varjani, R. Joshi, V. K. Srivastava, H. H. Ngo and W. Guo, *Environ. Sci. Pollut. Res.*, 2020, **27**, 27172–27180.
3 W.-W. Li and H.-Q. Yu, *Biotechnol. Adv.*, 2011, **29**, 972–982.
4 X. Zhang, W. He, L. Ren, J. Stager, P. J. Evans and B. E. Logan, *Bioresour. Technol.*, 2015, **176**, 23–31.
5 S. Varjani, G. Kumar and E. R. Rene, *J. Environ. Manage.*, 2019, **232**, 505–513.
6 S. Shokrollahzadeh, F. Golmohammad, N. Naseri, H. Shokouhi and M. Arman-Mehr, *Procedia Eng.*, 2012, **42**, 942–947.
7 M. Nasiri and I. Jafari, *Period. Polytech., Chem. Eng.*, 2017, **61**, 73–81.
8 N. Mintcheva, G. Gicheva and M. Panayotova, *Pollutants*, 2022, **2**, 234–251.
9 J. Lu, X. Wang, B. Shan, X. Li and W. Wang, *Chemosphere*, 2006, **62**, 322–331.
10 F. P. Perera, D. Tang, S. Wang, J. Vishnevetsky, B. Zhang, D. Diaz, D. Camann and V. Rauh, *Environ. Health Perspect.*, 2012, **120**, 921–926.
11 J. Jasmine and S. Mukherji, *J. Environ. Manage.*, 2015, **149**, 118–125.
12 C. Thakur, V. C. Srivastava, I. D. Mall and A. D. Hiwarkar, *Clean: Soil, Air, Water*, 2018, **46**, 1700624.
13 S. J. Varjani, R. R. Joshi, P. Senthil Kumar, V. K. Srivastava, V. Kumar, C. Banerjee and R. Praveen Kumar, *Waste bioremediation*, 2018, pp. 185–199.
14 G. Zafra, A. Moreno-Montaño, Á. E. Absalón and D. V. Cortés-Espinosa, *Environ. Sci. Pollut. Res.*, 2015, **22**, 1034–1042.
15 S. J. Varjani, E. Gnansounou and A. Pandey, *Chemosphere*, 2017, **188**, 280–291.
16 K. Sheth and K. V. Italia, *Int. j. innov. res. sci. technol.*, 2017, **4**, 56–59.
17 D. K. Tiwari, J. Behari and P. Sen, *World Appl. Sci. J.*, 2008, **3**, 417–433.
18 R. L. Droste and R. L. Gehr, *Theory and practice of water and wastewater treatment*, John Wiley & Sons, 2018.
19 S. K. Gupta, J. Behari and K. K. Kesari, *Asian J. Water, Environ. Pollut.*, 2006, **3**, 101–105.
20 P. Jangid and M. P. Inbaraj, *Mater. Today: Proc.*, 2021, **43**, 2877–2881.
21 I. Oller, S. Malato and J. Sánchez-Pérez, *Sci. Total Environ.*, 2011, **409**, 4141–4166.
22 L. Zhang and M. Fang, *Nano Today*, 2010, **5**, 128–142.
23 X. Dai, J. Fang, L. Li, Y. Dong and J. Zhang, *Int. J. Environ. Res. Public Health*, 2019, **16**, 3223.
24 A. Fakhru'l-Razi, A. Pendashteh, L. C. Abdullah, D. R. A. Biak, S. S. Madaeni and Z. Z. Abidin, *J. Hazard. Mater.*, 2009, **170**, 530–551.
25 M. Amil Usmani, I. Khan, A. H. Bhat, R. S. Pillai, N. Ahmad, M. K. Mohamad Haafiz and M. Oves, *Curr. Org. Synth.*, 2017, **14**, 206–226.
26 M. Super, H. D. V. Heese, D. MacKenzie, W. Dempster, J. Du Plessis and J. Ferreira, *Water Res.*, 1981, **15**, 1265–1270.
27 J. N. Kostraba, E. C. Gay, M. Rewers and R. F. Hamman, *Diabetes Care*, 1992, **15**, 1505–1508.
28 M. M. Dorsch, R. K. Scragg, A. J. McMichael, P. A. Baghurst and K. F. Dyer, *Am. J. Epidemiol.*, 1984, **119**, 473–486.
29 O. Aremu, C. Akintayo, E. Naidoo, S. Nelana and O. Ayanda, *Int. J. Environ. Sci. Technol.*, 2021, 1–20.
30 K. Gupta, S. Bhattacharya, D. Chattopadhyay, A. Mukhopadhyay, H. Biswas, J. Dutta, N. R. Ray and U. C. Ghosh, *Chem. Eng. J.*, 2011, **172**, 219–229.
31 M. E. Doyle, *Nanotechnology: a Brief Literature Review*, Food Research Institute, UW-Madison, 2006.
32 E. A. S. Dimapilis, C.-S. Hsu, R. M. O. Mendoza and M.-C. Lu, *Sustainable Environ. Res.*, 2018, **28**, 47–56.
33 P. R. S. Baabu, H. K. Kumar, M. B. Gumpu, J. Babu K, A. J. Kulandaisamy and J. B. B. Rayappan, *Materials*, 2022, **16**, 59.
34 N. Priya, K. Kaur and A. K. Sidhu, *Front. nanotechnol.*, 2021, **3**, 655062.
35 E. M. Mostafa and E. Amdeha, *Environ. Sci. Pollut. Res.*, 2022, **29**, 69861–69874.
36 A. Vakili, A. Zinatizadeh, Z. Rahimi, S. Zinadini, P. Mohammadi, S. Azizi, A. Karami and M. Abdulgader, *J. Cleaner Prod.*, 2023, **382**, 134899.
37 O. Bundit and K. Wongsaprom, *J. Phys.: Conf. Ser.*, 2018, **1144**, 012044.
38 P. Lahure, P. Salunke, R. Soliwal, A. Yadav, S. Tripathi and A. Koser, *Int. J. Sci. Res. Phys. Appl. Sci.*, 2015, **3**, 32–33.
39 M. Farahmandjou and F. Soflaee, *Phys. Chem. Res.*, 2015, **3**, 191–196.
40 A. B. Habtemariam and M. Maaza, 2022.
41 N. Chandrasekar, K. Kumar, K. S. Balasubramnian, K. Karunamurthy and R. Varadharajan, *Dig. J. Nanomater. Biostructures.*, 2013, **8**, 265.
42 H. T. Ha, P. T. Phong and T. D. Minh, *J. Anal. Methods Chem.*, 2021, **2021**, 1–9.
43 P. Kongsune, S. Rattanapan and R. Chanajaree, *Groundw. Sustain. Dev.*, 2021, **12**, 100524.
44 F. S. Awad, K. M. AbouZied, A. M. Bakry, W. M. Abou El-Maaty, A. M. El-Wakil and M. S. El-Shall, *J. Mater. Sci.*, 2021, **56**, 7982–7999.

45 F. S. Awad, K. M. AbouZied, W. M. Abou El-Maaty, A. M. El-Wakil and M. S. El-Shall, *Arabian J. Chem.*, 2020, **13**, 2659–2670.
46 H. I. Adegoke, F. AmooAdekola, O. S. Fatoki and B. J. Ximba, *Korean J. Chem. Eng.*, 2014, **31**, 142–154.
47 P. Xu, G. M. Zeng, D. L. Huang, C. L. Feng, S. Hu, M. H. Zhao, C. Lai, Z. Wei, C. Huang and G. X. Xie, *Sci. Total Environ.*, 2012, **424**, 1–10.
48 N. J. Bandara, J. P. A. Hettiaratchi, S. Wirasinghe and S. Pilapiiya, *Environ. Monit. Assess.*, 2007, **135**, 31–39.
49 X. Zhang, X. Dong, H. Huang, Y. Liu, W. Wang, X. Zhu, B. Lv, J. Lei and C. Lee, *Appl. Phys. Lett.*, 2006, **89**, 051101.
50 S. Hu and L. V. Wang, *Front. Neuroenerg.*, 2010, **2**, 1560.
51 M. Ozmen, K. Can, G. Arslan, A. Tor, Y. Cengeloglu and M. Ersoz, *Desalination*, 2010, **254**, 162–169.